6690 *Inorg. Chem.* **2010**, *49*, 6690–6696
DOI: 10.1021/ic100728s

Inorganic Chemistry
Article

Crystal Chemistry of the Potassium and Rubidium Uranyl Borate Families Derived from Boric Acid Fluxes

Shuao Wang,[†] Evgeny V. Alekseev,*[,†,‡] Jared T. Stritzinger,[†] Wulf Depmeier,[‡] and Thomas E. Albrecht-Schmitt*[,†]

[†]*Department of Civil Engineering and Geological Sciences and Department of Chemistry and Biochemistry, 156 Fitzpatrick Hall, University of Notre Dame, Notre Dame, Indiana 46556, and*
[‡]*Institut für Geowissenschaften, Universität zu Kiel, 24118 Kiel, Germany*

Received April 15, 2010

The reaction of uranyl nitrate with a large excess of molten boric acid in the presence of potassium or rubidium nitrate results in the formation of three new potassium uranyl borates, $K_2[(UO_2)_2B_{12}O_{19}(OH)_4]\cdot 0.3H_2O$ (**KUBO-1**), $K[(UO_2)_2B_{10}O_{15}(OH)_5]$ (**KUBO-2**), and $K[(UO_2)_2B_{10}O_{16}(OH)_3]\cdot 0.7H_2O$ (**KUBO-3**) and two new rubidium uranyl borates $Rb_2[(UO_2)_2B_{13}O_{20}(OH)_5]$ (**RbUBO-1**) and $Rb[(UO_2)_2B_{10}O_{16}(OH)_3]\cdot 0.7H_2O$ (**RbUBO-2**). The latter is isotypic with **KUBO-3**. These compounds share a common structural motif consisting of a linear uranyl, UO_2^{2+}, cation surrounded by BO_3 triangles and BO_4 tetrahedra to create an UO_8 hexagonal bipyramidal environment around uranium. The borate anions bridge between uranyl units to create sheets. Additional BO_3 triangles extend from the polyborate layers and are directed approximately perpendicular to the sheets. All of these compounds adopt layered structures. With the exception of **KUBO-1**, the structures are all centrosymmetric. All of these compounds fluoresce when irradiated with long-wavelength UV light. The fluorescence spectrum yields well-defined vibronically coupled charge-transfer features.

Introduction

Actinide oxoanion compounds continue to fascinate and mystify researchers by virtue of the remarkable variety of unusual structures that they can adopt,[1] and the vast array of properties that these compounds can display that include ion exchange,[2] mixed valency,[3] ionic conductivity,[4] enhanced fluorescence,[5] magnetic ordering,[6] and nonlinear optical properties.[7] These structures range from the extraordinary complexity of the uranium mineral Wölsendorfite, $Pb_{6.16}Ba_{0.36}[(UO_2)_{14}O_{19}(OH)_4](H_2O)_{12}$, whose layered topology is so complex that the length of the repeating *c* axis is nearly 56 Å[8] to both neutral and charged nanotubular structures adopted by uranyl phosphonates and selenates.[9] There are also compounds that are difficult to rival in terms of the variability of the coordination around the metal centers, such as in $Na_2Li_8[(UO_2)_{11}O_{12}(WO_5)_2]$, where UO_6, UO_7, and UO_8 tetragonal, pentagonal, and hexagonal bipyramids are all contained within one compound.[10] Mixed and intermediate valency are known in both uranium[3] and neptunium[11] compounds, and these materials

*E-mail: talbrec1@nd.edu.

(1) (a) Burns, P. C.; Miller, M. L.; Ewing, R. C. *Can. Mineral.* **1996**, *34*, 845. (b) Burns, P. C. In *Uranium: Mineralogy, Geochemistry and the Environment*; Burns, P. C., Finch, R., Eds.; Mineralogical Society of America: Washington, DC, 1999; Chpt. 1. (c) Burns, P. C. *Mater. Res. Soc. Symp. Proc.* **2004**, *802*, 89. (d) Burns, P. C. *Can. Mineral.* **2005**, *43*, 1839. (e) Krivovichev, S. V. *Structural Crystallography of Inorganic Oxysalts*: Oxford University Press, Oxford, U.K., 2009.

(2) (a) Dieckmann, G. H.; Ellis, A. B. *Solid State Ionics* **1989**, *32/33*, 50. (b) Vochten, R. *Am. Mineral.* **1990**, *75*, 221. (c) Benavente, J.; Ramos Barrado, J. R.; Cabeza, A.; Bruque, S.; Martinez, M. *Colloids Surf., A* **1995**, *97*, 13. (d) Shvareva, T. Y.; Almond, P. M.; Albrecht-Schmitt, T. E. *J. Solid State Chem.* **2005**, *178*, 499. (e) Shvareva, T. Y.; Sullens, T. A.; Shehee, T. C.; Albrecht-Schmitt, T. E. *Inorg. Chem.* **2005**, *44*, 300. (f) Shvareva, T. Y.; Skanthkumar, S.; Soderholm, L.; Clearfield, A.; Albrecht-Schmitt, T. E. *Chem. Mater.* **2007**, *19*, 132. (g) Ok, K. M.; Baek, J.; Halasyamani, P. S. *Inorg. Chem.* **2006**, *45*, 10207.

(3) (a) Lee, C.-S.; Wang, S.-L.; Lii, K.-H. *J. Am. Chem. Soc.* **2009**, *131*, 15116. (b) Lin, C.-H.; Lii, K.-H. *Angew. Chem., Int. Ed.* **2008**, *47*, 8711.

(4) (a) Grohol, D.; Blinn, E. L. *Inorg. Chem.* **1997**, *36*, 3422. (b) Johnson, C. H.; Shilton, M. G.; Howe, A. T. *J. Solid State Chem.* **1981**, *37*, 37. (c) Moreno-Real, L.; Pozas-Tormo, R.; Martinez-Lara, M.; Bruque-Gamez, S. *Mater. Res. Bull.* **1987**, *22*, 29. (d) Pozas-Tormo, R.; Moreno-Real, L.; Martinez-Lara, M.; Rodriguez-Castellon, E. *Can. J. Chem.* **1986**, *64*, 35. (e) Obbade, S.; Dion, C.; Saadi, M.; Abraham, F. *J. Solid State Chem.* **2004**, *177*, 1567. (f) S. Obbade, S.; Duvieubourg, L.; Dion, C.; Abraham, F. *J. Solid State Chem.* **2007**, *180*, 866.

(5) (a) Almond, P. M.; Talley, C. E.; Bean, A. C.; Peper, S. M.; Albrecht-Schmitt, T. E. *J. Solid State Chem.* **2000**, *154*, 635. (b) Frisch, M.; Cahill, C. L. *Dalton Trans.* **2006**, *39*, 4679. (c) Cahill, C. L.; de Lill, D. T.; Frisch, M. *CrystEngComm.* **2007**, *9*, 15.

(6) Almond, P. M.; Deakin, L.; Porter, M. O.; Mar, A.; Albrecht-Schmitt, T. E. *Chem. Mater.* **2000**, *12*, 3208.

(7) Sykora, R. E.; Albrecht-Schmitt, T. E. *Inorg. Chem.* **2003**, *47*, 2179.

(8) Burns, P. C. *Am. Mineral.* **1999**, *84*, 1661.

(9) (a) Poojary, D. M.; Grohol, D.; Clearfield, A. *Angew. Chem. Int. Ed.* **1995**, *34*, 1508. (b) Krivovichev, S. V.; Kahlenberg, V.; Tananaev, I. G.; Kaindl, R.; Mersdorf, E.; Myasoedov, B. F. *J. Am. Chem. Soc.* **2005**, *127*, 1072. (c) Alekseev, E. V.; Krivovichev, S. V.; Depmeier, W. *Angew. Chem., Int. Ed.* **2008**, *47*, 549.

(10) (a) Alekseev, E. V.; Krivovichev, S. V.; Depmeier, W.; Siidra, O. I.; Knorr, K.; Suleimanov, E. V.; Chuprunov, E. V. *Angew. Chem., Int. Ed.* **2006**, *45*, 7233. (b) Krivovichev, S. V.; Kahlenberg, V.; Tananaev, I. G.; Kaindl, R.; Mersdorf, E.; Myasoedov, B. F. *J. Am. Chem. Soc.* **2005**, *127*, 1072. (c) Albrecht-Schmitt, T. E. *Angew. Chem., Int. Ed.* **2005**, *44*, 4836.

(11) Almond, P. M.; Sykora, R. E.; Skanthakumar, S.; Soderholm, L.; Albrecht-Schmitt, T. E. *Inorg. Chem.* **2004**, *43*, 958.

Published on Web 06/18/2010

combine both unprecedented structures with atypical electronic properties.

One family of actinide oxoanion compounds that is poorly explored is the actinide borates. This is surprising for several reasons, the first of which is that a thorium borate was reported in 1826 by Berzelius.[12] Credible examples of well-defined actinide borates were absent until the 1980s when a series of crystal structures were reported for uranyl borates.[13−18] These compounds were all synthesized via high-temperature B_2O_3 melt reactions above 1000 K. These compounds share a common motif in that the boron atoms are typically found to have the BO_3 triangular configuration, which is more thermodynamically favorable than BO_4 tetrahedra at high temperatures. The single exception to this is the molecular system, $K_6[UO_2\{B_{16}O_{24}(OH)_8\}]\cdot 12H_2O$, which was prepared at room temperature via slow evaporation[19] and is composed of a cyclic cluster of BO_3 and BO_4 units with a central uranyl core. A single crystallographically characterized thorium borate, ThB_2O_5, can be added to this list.[20] After these initial studies, additional actinide borates were not reported for 20 years.

Actinide borates are difficult to synthesize via commonly employed techniques, such as hydrothermal reactions, because water competes very successfully with borate for inner-sphere coordination sites with these metals under most conditions. Our strategy for preparing actinide borates is to capitalize on low-temperature boric acid flux reactions that have yielded a thorium borate, $[ThB_5O_6(OH)_6][BO(OH)_2]\cdot 2.5H_2O$ (**NDTB-1**), with a cationic framework structure and a remarkable anion exchange capabilities,[21] a large family of uranyl borates,[22,23] three mixed-valent neptunium borates,[24,25] and a single plutonium(VI) borate, which is similar to its uranium counterparts.[24] We have shown that boric acid fluxes are an excellent medium for preparing actinide borates in general. These conditions yield completely new coordination environments and topologies for actinide compounds.[21−25] In addition, a significant percentage of uranyl borates adopt noncentrosymmetric structures, and these compounds may aid in the design of nonlinear optical materials. In this paper, we substantially expand the uranyl borate family to include compounds that contain potassium and rubidium. These cations can yield structural features that have not been observed with other cations and provide important insights into how subtle changes in composition can lead to dramatic changes in properties.

(12) Berzelius, J. J. *Pogg. Ann.* **1826**, *16*, 385.
(13) Gasperin, M. *Acta Crystallogr.* **1987**, *C43*, 1247.
(14) Gasperin, M. *Acta Crystallogr.* **1987**, *C43*, 2031.
(15) Gasperin, M. *Acta Crystallogr.* **1987**, *C43*, 2264.
(16) Gasperin, M. *Acta Crystallogr.* **1988**, *C44*, 415.
(17) Gasperin, M. *Acta Crystallogr.* **1989**, *C45*, 981.
(18) Gasperin, M. *Acta Crystallogr.* **1990**, *C46*, 372.
(19) Behm, H. *Acta Crystallogr.* **1985**, *C41*, 642.
(20) Gasperin, M. *Acta Crystallogr.* **1991**, *C47*, 10.
(21) Wang, S.; Alekseev, E. V.; Diwu, J.; Casey, W. H.; Phillips, B. L.; Depmeier, W.; Albrecht-Schmitt, T. E. *Angew. Chem., Int. Ed.* **2010**, *49*, 1057.
(22) Wang, S.; Alekseev, E. V.; Ling, J.; Liu, G.; Depmeier, W.; Albrecht-Schmitt, T. E. *Chem. Mater.* **2010**, *22*, 2155.
(23) Wang, S.; Alekseev, E. V.; Stritzinger, J. T.; Depmeier, W.; Albrecht-Schmitt, T. E. *Inorg. Chem.* **2010**, *49*, 2948.
(24) Wang, S.; Alekseev, E. V.; Ling, J.; Skanthakumar, S.; Soderholm, L.; Depmeier, W.; Albrecht-Schmitt, T. E. *Angew. Chem., Int. Ed.* **2010**, *49*, 1263.
(25) Wang, S.; Alekseev, E. V.; Depmeier, W.; Albrecht-Schmitt, T. E. *Chem. Commun.* **2010**, *46*, 3955.

Experimental Section

Syntheses. $UO_2(NO_3)_2\cdot 6H_2O$ (98%, International Bio-Analytical Industries), H_3BO_3 (99.99%, Alfa-Aesar), KNO_3 (99.3%, Aldrich), and $RbNO_3$ (99.8%, Alfa-Aesar) were used as received without further purification. Distilled and Millipore filtered water with a resistance of 18.2 MΩ·cm was used in all reactions. PTFE-lined autoclaves were used for all reactions. While the $UO_2(NO_3)_2\cdot 6H_2O$ used in this study contained depleted U, there are really not many compositional or radiological differences between depleted and natural abundance uranium, and standard precautions for handling radioactive materials should be followed at all times. There are very old sources of uranyl nitrate that may not be depleted, and enhanced care is warranted for these samples.

Synthesis of $K_2[(UO_2)_2B_{12}O_{19}(OH)_4]\cdot 0.3H_2O$ (KUBO-1), $K[(UO_2)_2B_{10}O_{15}(OH)_5]$ (KUBO-2), and $K[(UO_2)_2B_{10}O_{16}(OH)_3]\cdot 0.7H_2O$ (KUBO-3). $UO_2(NO_3)_2\cdot 6H_2O$, boric acid, potassium nitrate with 10 different K:U:B molar ratios (1:1:6, 1:1:10, 1:1:15, 2:1:8, 2:1:15, 3:1:8, 3:1:15, 4:1:15, 5:1:15, and 6:1:15) (1 mmol of $UO_2(NO_3)_2\cdot 6H_2O$ was used in each potassium and rubidium reaction) were loaded into 10,23 mL autoclaves. The autoclaves were sealed and heated to 190 °C in a box furnace for 24 h. The autoclaves were then cooled down to room temperature at a rate of 5 °C/h. All the products were washed with boiling water to remove excess boric acid, followed by rinsing with methanol. Crystals in the form of tablets with light yellow-green coloration were collected for all reactions. The tablets of **KUBO-1** are remarkably well-formed triangles. The same conditions and procedures were used for both the potassium and rubidium reactions. Single-crystal and powder X-ray diffraction studies reveal that **KUBO-2** forms as the major product of the first six ratios, except for the 2:1:8 reaction where it is a minor product, it also exists in the 3:1:8 and 3:1:15 reactions. **KUBO-3** forms in the 2:1:8 reaction as the major product and in the 2:1:15, 3:1:8, 3:1:15 reactions as the minor product. **KUBO-1** only occurs in high-K^+ ratio reactions for last five ratios and can be found as a pure phase for the last three reaction ratios.

Synthesis of $Rb_2[(UO_2)_2B_{13}O_{20}(OH)_5]$ (RbUBO-1) and $Rb[(UO_2)_2B_{10}O_{16}(OH)_3]\cdot 0.7H_2O$ (RbUBO-2). RbUBO-1 can be prepared using $UO_2(NO_3)_2\cdot 6H_2O$, boric acid, rubidium nitrate at Rb:U:B molar ratio of 5:1:15. **RbUBO-2** can be made in the reaction with a ratio of 2:1:15. Crystals in the form of tablets were isolated from the first reaction and blocks for the second reaction. The crystals have light yellow-green coloration.

Crystallographic Studies. Single crystals of all five **KUBO** and **RbUBO** phases were mounted on glass fibers and optically aligned on either a Bruker APEXII CCD or a Bruker APEXII Quazar X-ray diffractometer using a digital camera. Initial intensity measurements were performed using a IμS X-ray source, a 30 W microfocused sealed tube (Mo Kα, λ = 0.71073 Å) with high-brilliance and high-performance focusing Quazar multilayer optics, or a standard sealed tube with a monocapillary collimator. Standard APEXII software was used for determination of the unit cells and data collection control. The intensities of reflections of a sphere were collected by a combination of four sets of exposures (frames). Each set had a different φ angle for the crystal, and each exposure covered a range of 0.5° in ω. A total of 1464 frames were collected with an exposure time per frame of 10−30 s, depending on the crystal. The SAINT software was used for data integration including Lorentz and polarization corrections. Semiempirical absorption corrections were applied using the program SADABS. Selected crystallographic data are listed in Table 1. Selected bond distances are given in Tables 2−5. Atomic coordinates, bond distances, and additional structural information are provided in the Supporting Information (CIF's).

The crystal structure of the **KUBO-3** is not publishable owing to nonmerohedral twinning. We have tried several crystals from

Table 1. Crystallographic Data for **KUBO-1**, **KUBO-2**, **RbUBO-1**, and **RbUBO-2**

compound	**KUBO-1**	**KUBO-2**	**RbUBO-1**	**RbUBO-2**
mass	1115.98	1007.26	1251.53	1048.83
color and habit	yellow-green, triangle tablet	yellow-green, tablet	yellow-green, tablet	yellow-green, block
space group	$P3_112$	$C2/c$	$P2_1/n$	$P2_1/m$
a (Å)	6.4418(4)	6.4637(4)	6.4449(3)	6.4063(7)
b (Å)	6.4418(4)	11.1151(7)	11.0969(5)	26.028(3)
c (Å)	47.457(3)	25.4185(16)	33.9974(16)	6.4573(7)
α (°)	90	90	90	90
β (°)	90	96.3710(10)	92.2595(5)	119.7160(10)
γ (°)	120	90	90	90
V (Å^3)	1705.47(18)	1814.9(2)	2429.55(19)	935.10(17)
Z	3	4	4	2
T (K)	293(2)	293(2)	293(2)	296(2)
λ (Å)	0.71073	0.71073	0.71073	0.71073
max 2θ (°)	28.92	28.62	28.78	28.75
ρcalcd (g cm^{-3})	3.260	3.686	3.422	3.725
μ(Mo Kα)	147.16	181.82	174.24	200.06
$R(F)$ for $F_0^2 > 2\sigma(F_0^2)^a$	0.0212	0.0407	0.0419	0.0403
$Rw(F_0^2)^b$	0.0552	0.1027	0.0917	0.0864

^{a} $R(F) = \sum\|F_0| - |F_c\|/\sum|F_0|$. ^{b} $R(F_0^2) = [\sum w(F_0^2 - F_c^2)^2/\sum w(F_0^4)]^{1/2}$.

Table 2. Selected Bond Distances (Å) for **KUBO-1**

bond	distance (Å)	bond	distance (Å)	bond	distance (Å)
U(1)−O(1)	1.759(3)	B(1)−O(3)	1.346(6)	B(4)−O(3)	1.481(7)
U(1)−O(2)	1.777(3)	B(1)−O(6)	1.346(6)	B(4)−O(4)	1.482(6)
U(1)−O(7)	2.409(4)	B(1)−O(8)	1.403(6)	B(5)−O(10)	1.461(7)
U(1)−O(4)	2.415(3)	B(2)−O(9)	1.356(7)	B(5)−O(4)	1.465(7)
U(1)−O(5)	2.417(3)	B(2)−O(11)	1.374(7)	B(5)−O(6)	1.472(7)
U(1)−O(8)	2.524(4)	B(2)−O(10)	1.386(7)	B(5)−O(7)	1.487(6)
U(1)−O(3)	2.581(3)	B(3)−O(13)	1.355(8)	B(6)−O(12)	1.450(7)
U(1)−O(6)	2.612(4)	B(3)−O(14)	1.361(10)	B(6)−O(5)	1.466(7)
		B(3)−O(12)	1.358(9)	B(6)−O(7)	1.477(7)
		B(4)−O(9)	1.440(6)	B(6)−O(8)	1.504(6)
		B(4)−O(5)	1.466(6)		

Table 3. Selected Bond Distances (Å) for **KUBO-2**

bond	distance (Å)	bond	distance (Å)	bond	distance (Å)
U(1)−O(2)	1.775(6)	B(1)−O(9)	1.363(11)	B(3)−O(11)	1.498(12)
U(1)−O(1)	1.764(6)	B(1)−O(7)	1.365(12)	B(3)−O(10)	1.476(12)
U(1)−O(3)	2.408(6)	B(1)−O(8)	1.364(12)	B(4)−O(3)	1.455(11)
U(1)−O(5)	2.414(5)	B(2)−O(6)	1.344(13)	B(4)−O(10)	1.448(12)
U(1)−O(10)	2.416(6)	B(2)−O(12)	1.406(13)	B(4)−O(9)	1.474(11)
U(1)−O(9)	2.557(6)	B(2)−O(11)	1.363(13)	B(4)−O(4)	1.490(11)
U(1)−O(8)	2.559(6)	B(3)−O(5)	1.465(11)	B(5)−O(6)	1.463(11)
U(1)−O(7)	2.628(6)	B(3)−O(7)	1.441(13)	B(5)−O(3)	1.447(11)
				B(5)−O(8)	1.471(11)
				B(5)−O(5)	1.497(12)

two different syntheses but all of them contained two twinning components. We used the Bruker software package (Cell_Now) for component separation, HKLF5 file creation, and structure refinement. Using the HKLF5 file, we obtained a final R_1 value of 2.87%, but unfortunately the displacement of two boron atoms were not well refined. The structure model of **KUBO-3** is similar with that of **RbUBO-2**, but it crystallizes in triclinic symmetry (space group $P\bar{1}$, unit cell parameters: a = 6.436(1), b = 6.437(1), and c = 13.051(2) Å and α = 84.548(2)°, β = 86.133(2)°, and γ = 60.083(2)°. The powder X-ray diffraction data and unit cell parameters comparison (c parameter in **RbUBO-2** is approximately 2*c in **KUBO-3**) also confirming isotypism of **RbUBO-2** and **KUBO-3**.

Powder X-ray Diffraction. Powder X-ray diffraction patterns of the products of all **KUBO** reactions were collected on a Scintag $\theta-\theta$ diffractometer equipped with a diffracted beamed monochromatic set for Cu Kα (λ = 1.54056 Å) radiation at room temperature in the angular range from 10° to 80° (2θ), with a scanning step width of 0.05° and a fixed counting time of 1 s/step. The collected patterns were compared with those calculated from single-crystal data using ATOMS (see Supporting Information).

UV−vis-NIR and Fluorescence Spectroscopy. UV−vis-NIR data were acquired from single crystals using a Craic Technologies microspectrophotometer. Crystals were placed on quartz slides under oil, and the data were collected from 200 to 1700 nm. Fluorescence data were obtained using 365 nm light for excitation.

Results and Discussion

Syntheses. The formation of three phases in the **KUBO** system is found to be a stoichiometrically driven reaction, which means that the formation of the four compounds is related to the molar ratio of potassium, uranium, and boron in the starting materials. The **KUBO-2** and **KUBO-3** phases possess a K:U ratio of 1:2 and are favored in the

Table 4. Selected Bond Distances (Å) for **RbUBO-1**

bond	distance (Å)	bond	distance (Å)	bond	distance (Å)
U(1)−O(1)	1.765(6)	B(1)−O(13)	1.361(11)	B(9)−O(14)	1.465(11)
U(1)−O(6)	1.774(6)	B(1)−O(12)	1.368(11)	B(9)−O(11)	1.465(11)
U(1)−O(11)	2.400(6)	B(1)−O(10)	1.374(12)	B(9)−O(7)	1.496(11)
U(1)−O(3)	2.400(6)	B(2)−O(17)	1.348(11)	B(10)−O(20)	1.457(11)
U(1)−O(16)	2.410(6)	B(2)−O(7)	1.369(11)	B(10)−O(16)	1.461(11)
U(1)−O(10)	2.511(6)	B(2)−O(18)	1.376(11)	B(10)−O(18)	1.464(11)
U(1)−O(17)	2.572(6)	B(3)−O(27)	1.352(13)	B(10)−O(3)	1.478(11)
U(1)−O(18)	2.582(6)	B(3)−O(25)	1.375(13)	B(11)−O(14)	1.448(11)
U(2)−O(4)	1.765(6)	B(3)−O(15)	1.384(13)	B(11)−O(12)	1.460(11)
U(2)−O(5)	1.765(6)	B(4)−O(23)	1.365(12)	B(11)−O(27)	1.467(11)
U(2)−O(14)	2.389(6)	B(4)−O(20)	1.367(12)	B(11)−O(2)	1.500(11)
U(2)−O(9)	2.391(6)	B(4)−O(21)	1.368(12)	B(12)−O(24)	1.445(11)
U(2)−O(2)	2.438(6)	B(5)−O(8)	1.338(12)	B(12)−O(9)	1.470(11)
U(2)−O(7)	2.562(6)	B(5)−O(26)	1.353(12)	B(12)−O(3)	1.472(11)
U(2)−O(13)	2.571(6)	B(5)−O(19)	1.384(12)	B(12)−O(13)	1.494(11)
U(2)−O(12)	2.579(6)	B(6)−O(29)	1.34(2)	B(13)−O(15)	1.436(11)
		B(6)−O(21)	1.38(2)	B(13)−O(2)	1.470(11)
		B(6)−O(22)	1.43(2)	B(13)−O(11)	1.479(11)
		B(7)−O(24)	1.343(14)	B(13)−O(17)	1.495(11)
		B(7)−O(28)	1.378(17)	B(8)−O(23)	1.465(11)
		B(7)−O(25)	1.396(15)	B(8)−O(10)	1.471(11)
		B(8)−O(9)	1.435(11)	B(8)−O(16)	1.480(12)
				B(9)−O(8)	1.455(11)

Table 5. Selected Bond Distances (Å) for **RbUBO2**

bond	distance (Å)	bond	distance (Å)	bond	distance (Å)
U(1)−O(6)	1.759(6)	B(1)−O(11)	1.349(9)	B(3)−O(9)	1.472(10)
U(1)−O(10)	1.773(6)	B(1)−O(4)	1.367(10)	B(3)−O(8)	1.485(10)
U(1)−O(7)	2.382(5)	B(1)−O(5)	1.388(10)	B(4)−O(7)	1.451(11)
U(1)−O(9)	2.405(5)	B(2)−O(3)	1.356(11)	B(4)−O(3)	1.454(11)
U(1)−O(8)	2.447(5)	B(2)−O(2)	1.356(11)	B(4)−O(9)	1.480(9)
U(1)−O(11)	2.547(5)	B(2)−O(1)	1.369(11)	B(4)−O(11)	1.483(10)
U(1)−O(4)	2.584(5)	B(3)−O(5)	1.458(9)	B(5)−O(8)	1.422(10)
U(1)−O(5)	2.587(6)	B(3)−O(2)	1.460(11)	B(5)−O(7)	1.462(10)
				B(5)−O(4)	1.483(10)
				B(5)−O(12)	1.491(12)

reactions that have a lower K:U ratio. When increased amounts of potassium are present in the reaction mixture, **KUBO-1**, which has a higher K:U ratio of 1:1, becomes more favored and can be made as a pure phase. The reaction yields increase with reaction time. One day reactions are appropriate for screening product composition but only lead to low isolated yields. The yield maximizes after three days at 57% for **KUBO-1** in reaction of K:U:B = 5:1:15. The two **RbUBO** phases are more difficult to prepare. Both of the RbUBO phases cannot be obtained as pure phases, and they always appear as minor products of the reaction along with β-$UO_2B_2O_4$ as the major product.

Crystal Structures and Some General Topological Aspects. Portions of the crystal structures of **KUBO-1**, **KUBO-2**, **RbUBO-1**, and **RbUBO-2** are shown in Figure 1. The crystal structures of all of the obtained phases are based on two-dimensional (2D) borate sheets with similar topologies. In the structures of four of the phases (**KUBO-1**, **KUBO-3**, **RbUBO-1**, and **RbUBO-2**), these sheets are linked into double layers by BO_3 triangles. In contrast, the structure of **KUBO-2** is based on single layers. In all of the uranium borates, the uranium centers are contained within uranyl groups, UO_2^{2+}, which are incorporated into the borate sheets. The resulting coordination of uranium atoms is as UO_8 hexagonal bipyramids.

KUBO-1. KUBO-1 is based on double, negatively charged layers united in a regular 3D structure by potassium cations distributed in the interlayer space (see Figure 1a). Each double layer has a thickness of about 15.5 Å. The single sheets within the double layers in **KUBO-1** have the **A** and **B** (in this case in form of **B′**) types of topologies which were earlier founded in

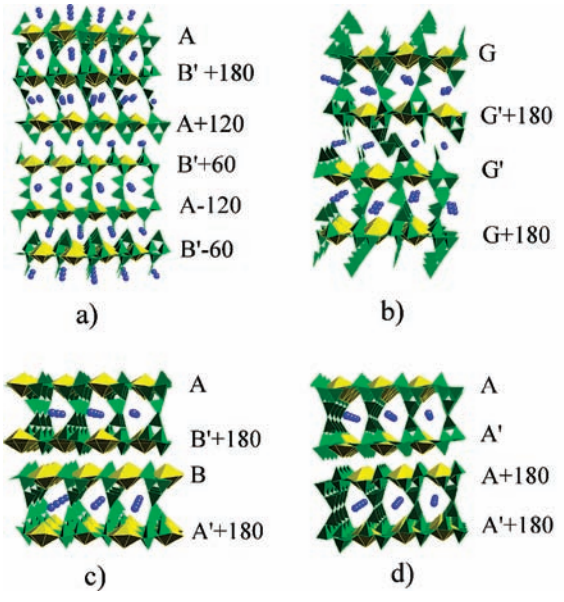

Figure 1. Views of the crystal structures of: **KUBO-1** (a), **RbUBO-1** (b), **KUBO-2** (c),and **RbUBO-2** and **KUBO-3** (d). UO_8 hexagonal bipyramids are shown in yellow, BO_3 and BO_4 units in green, and K^+ and Rb^+ cations in blue.

pure uranyl borates and sodium uranyl borate systems.[22,23] This topology is based on a single BO_3 group linked with three groups each consisting of three BO_4 tetrahedra. This is the simplest topology we found in actinide borates. Each double layer consists of both types (**A** and **B**′) of borate sheets. The sheets are linked into double layers by two BO_3 triangles (B_2O_5 groups) which act as columns, and the structures could be considered as being pillared. These groups are titled away from the plane of the sheets because sheets are slightly shifted within one double layer with respect to each other (Figure 1a). This tilting and shifting reduces the interlayer space. The potassium cation and water molecule sites are in the pores of doubled layers between the B_2O_5 groups and the borate sheets. These positions are split and partially occupied because of a high volume of free space in the cavities (the same situation occurs in **RbUBO-1**). The single BO_3 triangles create a sawtooth-like configuration on the periphery of the double layers. Each double layer in the structure of **KUBO-1** is rotated by 120° compared to the next layer. This is clearly visible from the single sheets positions in Figure 1. Because of this orientational change three double layers exist in one unit cell with a total of 360° of turning, which is equivalent to a translation element. As we mentioned, one layer in **KUBO-1** has 15.5 Å thickness, and as result, we have a long unit cell parameter of $c = 47.747(3)$ Å (Table 1).

KUBO-2. This potassium uranyl borate has an identical chemical composition with α-$Na[(UO_2)_2B_{10}O_{15}(OH)_5]$] (**NaUBO-1**) and β-$Na[(UO_2)_2B_{10}O_{15}(OH)_5]$ (**NaUBO-2**) and is related with the hydrated compound, $Na[(UO_2)_2B_{10}O_{15}(OH)_5]\cdot 3H_2O$ (**NaUBO-3**).[22] The crystal structures of these phases are also quite similar (Figure 1c). The structure of these compounds are based on 2D single layers constructed from polymerized borate clusters with **A** (**A**′) and **B** (**B**′) topologies. The layers rotated by 180° with respect to each other. The additional BO_3 triangle groups are only on one side of borate single sheets. These groups are directed into one side of the neighboring layers (Figure 1c), and as result, a quasidoubled layer results without real linkages between the BO_3 groups. The potassium cations are in the voids between the single layers on the side where the BO_3 triangles are. The connection of the layers is provided by K^+ cations (in the places where they are) and by hydrogen bonds (on the opposite sides of single layers).

Chemically and topologically **KUBO-2**, **NaUBO-1**, and **NaUBO-2** are practically identical. The main difference between them is in the ordering and orientation of **A** (**A**′) and **B** (**B**′) sheet types. In the sodium phases, we have found **A**/**A**′/**B**/**B**′ and **B**/**B**′/**B**/**B**′ packing (in **NaUBO-1** and **NaUBO-2,** respectively), but in the potassium phases, the packing type is different, A/B′/B/A′. These differences produced differences in the number of layers in the unit cell and in the alkali metal cation environments.

RbUBO-1. The rubidium uranyl borate **RbUBO-1** has the most complicated crystal structure and a different borate sheet topology and is shown in Figure 1b. In general this structure is similar with structure of **KUBO-1** because it is also based on doubled layers consisting of single borate sheets. However, these sheets are slightly different from **A**/**A**′/**B**/**B**′-type topology, and they are based on a superposition of them. The schematic representation of the borate sheets in **RbUBO-1** is given in Figure 2a. The sheets as in the **A** and **B** types are based on flat BO_3 triangles linked by corners with the super triangular groups.

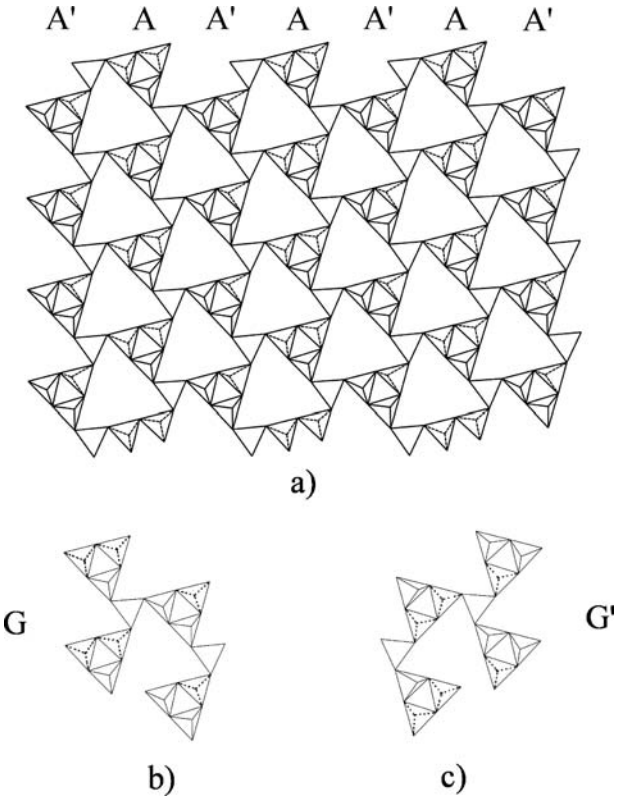

Figure 2. A skeletal representation of the polyborate sheet found in the structure of **RbUBO-1**: general view (a) and detailed view of two possible configurations (b) and (c).

These super triangular groups consist of three BO_4 tetrahedra. Two of them are directed toward one side ("up" or "down"), and the third is directed opposite to them. In the structure of the **A**- and **B**-type sheets, all three super triangles (surrounding flat BO_3 triangles) have the same internal structure (for example two tetrahedrons "up" and one "down" in structure of **A**′ and **B**′). In the structure of **RbUBO-1**, this order is not retained. In Figure 2a, it is shown that each single BO_3 triangle is interconnected with two identical super triangles (with identical internal structure) and one group with reversed structure. As the result of this a single triangle BO_3 cannot be used for the topological description of the sheets in **RbUBO-1**. The topology of these new layers is referred to as **G** in this work (after **E** and **F**) by the environment of the two neighboring BO_3 groups as is shown in Figure 2b and c. The resulting topology of the **G** sheets is based on alternating **A** and **A**′ or **B** and **B**′ fragments, as is shown in Figure 2a. Because in one sheet there exists both variants of the orientation of the supertriangles, the **G**-type sheet is not enantiomorphic. Transformation from the **G** conformation to **G**′ can be made by simple rotation around of the two-fold axis in the figure plane (Figure 2a). This is the first example of this sheet topology construction by combination of previously known topologies of uranyl borate phases. The topologies of other non-A/B or -C/D sheets were combined from Np/Pu borates sheets topologies.[24]

Each sheet, described above, within one layer is rotated by 180° in comparison with the other. The sheets linked by B_2O_5 groups into double layers (Figure 1b). In contrast with **KUBO-1**, where B_2O_5 groups are linked with the sheets at two points (Figure 1a), the B_2O_5 groups in

RbUBO-1 are linked with sheets at three locations. The free space within one layer (between single sheets) is filled by Rb^+ cations, which partially compensate for the negative charge of the layers. The rubidium atoms positions within the layers are split between two sites, which are partially occupied in the same manner as in **KUBO-1**. The outer sides of double layers are covered by two types of groups, BO_3 single triangle and B_2O_5 dimers. These groups form an optimal environment for the Rb^+ cations in the interlayer space. The Rb atoms in the interlayer space are providing the interconnection of the double layers as the potassium cations do in **KUBO-1**. Thus both structures are similar in packing (double layers, B_2O_5 as sheet linkers and A^+ cations within and outside of the layers), but the difference in the ionic radius of K^+ and Rb^+ directs the structural fragments in different ways.

RbUBO-2 and KUBO-3. The phases **RbUBO-2** and **KUBO-3** have the same chemical compositions and are isotypic. Here only the Rb phase is described because all of the potassium-containing crystals from several syntheses were twinned in a manner that could be resolved (but structure was solved and refined). A portion of the **RbUBO-2** crystal structure is shown in Figure 1d. This structure is related to both of the previously described packing types, double layers from **KUBO-1** and **RbUBO-1** and "free" interlayer space as in **KUBO-2**. The double layers in **KUBO-3** and **RbUBO-2** are linked by B_2O_5 dimers with four points of connections to the single borate sheets. Here we see the difference from the linking of borate sheets by B_2O_5 in **KUBO-1** (two points of connection) and **RbUBO-1** (three points of connection). As a result, projections of the single sheets within one double layer are identical without any kind of shift. The difference is only in the topology of the sheets, **A**/**A**′, and the rotation of the next double layers by 180° (Figure 1d). There are not any additional groups (BO_3 or B_2O_5) on the outer side of double layers. This makes the structure of **KUBO-3** and **RbUBO-2** closer to the structure of **KUBO-2**. The structures of **KUBO-3** and **RbUBO-2** can be presented as a result of **KUBO-2** structure condensation: **KUBO-2** → **KUBO-3** + H_2O. This is clearly visible from structure comparison (Figure 1c and d); the single BO_3 triangles terminate with OH groups (in **KUBO-2**) and are condensed to B_2O_5 dimers (in **KUBO-3** and **RbUBO-2**). Such processes are well-known in layered silicate precursors for zeolite-type materials.[26]

Fluorescence Properties of Potassium and Rubidium Uranyl Borates. The term "fluorescence" was first coined in the late 1700s in France to describe the green glow from uranyl salts that occurs when natural light irradiates them. This emission is in fact highly complex and is a strong vibronically coupled charge-transfer emission. Emission from uranyl compounds has been carefully and extensively studied, especially by Denning and co-workers, who assigned all of the vibronic transitions from single crystals containing the $[UO_2Cl_4]^{2-}$ anion.[27] While it is generally thought that five broad features centered near 520 nm are generally observed for uranyl compounds at room temperature, far more bands are observed at low temperatures.

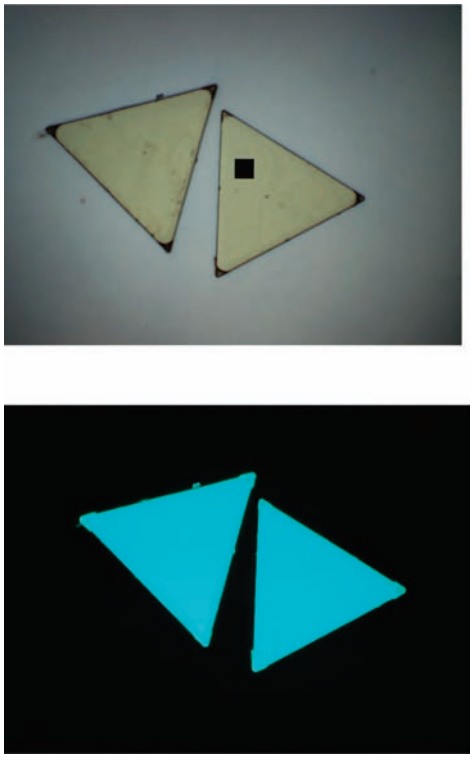

Figure 3. Single crystals of **KUBO-1** showing their triangular habit (top). The black square aperture (size 6.3 × 6.3 μm) indicates the scale. The same crystals under irradiation with 365 nm light (bottom).

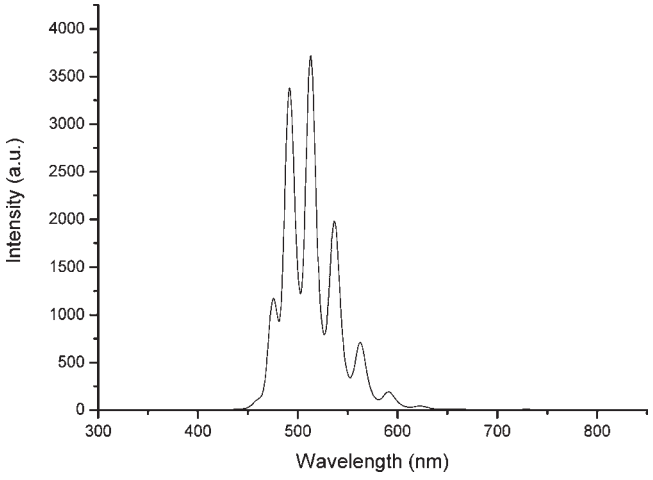

Figure 4. Fluorescence spectrum of **KUBO-1** showing vibronically coupled charge-transfer bands.

KUBO-1 forms rather remarkable triangular tablets with a pale yellow-green coloration. Upon irradiation with 365 nm light, the crystals fluoresce with sufficient intensity that the emission from a few crystals is easily observed by the naked eye, as shown in Figure 3. The fluorescence spectrum of this compound shows very narrow features for a room temperature spectrum, and the five typical vibronic bands are observed as shown in Figure 4. However, three additional weaker features can

(26) (a) Oberhagemann, U.; Bayat, P.; Marler, B.; Gies, H.; Rius, J. *Angew. Chem., Int. Ed.* **2003**, *35*, 2869. (b) Li, Z.; Marler, B.; Gies, H. *Chem. Mater.* **2008**, *20*, 1896.

(27) Denning, R. G.; Norris, J. O. W.; Short, I. G.; Snellgrove, T. R.; Woodwark, D. R. *Lanthanide and Actinide Chemistry and Spectroscopy*; Edelstein, N. M., Ed; ACS Symposium Series no. 131; American Chemical Society: Washington, DC, 1980; Chapter 15.

be clearly identified in this spectrum. The resolution of these additional features and the sharpness of the spectrum can probably be attributed to the remarkable quality of the crystals of this compound.[28] All of the compounds described in this work yield fluorescence spectra similar to that shown in Figure 4.

Conclusions

Uranyl borates derived from boric acid fluxes have yielded a total of seven different sheet topologies thus far despite the fact that they are all a combination of the same three building units, UO_8 hexagonal bipyramids, BO_3 triangles, and BO_4 tetrahedra. These sheets invariably possess additional BO_3 triangles that extend into the interlayer space. In some cases these groups separate the layers, and in others they join them together to yield double layers or three-dimensional frameworks. The structures are typically noncentrosymmetric and are often polar. The interlayer cations play structure-directing roles, and the size of the cations affects the type of structure achieved. Finally, product composition, which is highly variable, is greatly influenced by reaction stoichiometry. In short, the uranyl borate system is one of the most complex actinide systems ever recorded.

Owing to the presence of the uranyl cations within the layers, all of these compounds fluoresce with sufficient intensity to be observed by the naked eye. The emission spectra show well-resolved vibronic coupling, and more features are observed for these compounds than are generally found, perhaps because the boric acid flux yields crystals of higher than normal quality. Other properties have also been observed, such as second-harmonic generation of laser light. Therefore, the structure−property relationships in this family are also quite rich and potentially useful.

Acknowledgment. We are grateful for support provided by the Chemical Sciences, Geosciences, and Biosciences Division, Office of Basic Energy Sciences, Office of Science, Heavy Elements Program, U.S. Department of Energy under Grant DE-FG02-01ER16026 and by Deutsche Forschungsgemeinschaft for support within the DE 412/43-1 research project. This material is based upon work supported as part of the Materials Science of Actinides, an Energy Frontier Research Center funded by the U.S. Department of Energy, Office of Science, Office of Basic Energy Sciences under Award Number DE-SC0001089. The National Science Foundation also supported a portion of this work through the REU program in solid-state and materials chemistry (DMR).

Supporting Information Available: X-ray crystallographic files for $K_2[(UO_2)_2B_{12}O_{19}(OH)_4]\cdot 0.3H_2O$ (**KUBO-1**), $K[(UO_2)_2B_{10}O_{15}(OH)_5]$ (**KUBO-2**), $Rb_2[(UO_2)_2B_{13}O_{20}(OH)_5]$ (**RbUBO-1**), and $Rb[(UO_2)_2B_{10}O_{16}(OH)_3]\cdot 0.7H_2O$ (**RbUBO-2**). Powder diffraction data for all of the reactions products are also given. This material is available free of charge via the Internet at http://pubs.acs.org.

(28) Liu, G.; Beitz, J. V. In *The Chemistry of the Actinide and Transactinide Elements*; Morss, L. R., Edelstein, N. M., Fuger, J., Eds.; Springer: Heidelberg, Germany, 2006; pp 2088.